# π–Hydrogen Bonding Wins over Conventional Hydrogen Bonding Interaction: A Jet-Cooled Study of Indole···Furan Heterodimer

**ARTICLE** *in* THE JOURNAL OF PHYSICAL CHEMISTRY A · FEBRUARY 2012

Impact Factor: 2.69 · DOI: 10.1021/jp211366z · Source: PubMed



**3 AUTHORS**, INCLUDING:

Sumit Kumar
Indian Institute of Science Education and Res…
**9** PUBLICATIONS **72** CITATIONS
SEE PROFILE

Aloke Das
Indian Institute of Science Education and Res…
**34** PUBLICATIONS **247** CITATIONS
SEE PROFILE

THE JOURNAL OF PHYSICAL CHEMISTRY A

Article

pubs.acs.org/JPCA

# π-Hydrogen Bonding Wins over Conventional Hydrogen Bonding Interaction: A Jet-Cooled Study of Indole···Furan Heterodimer

Sumit Kumar, Vedant Pande, and Aloke Das*

Department of Chemistry, Indian Institute of Science Education & Research (IISER), 900 NCL Innovation Park, Dr. Homi Bhabha Road, Pune-411008, Maharashtra, India

Supporting Information

**ABSTRACT:** In this study, we have explored the conformational landscape of the indole···furan dimer in a supersonic jet by using resonant two-photon ionization (R2PI) and IR-UV double-resonance spectroscopic techniques combined with dispersion-corrected density functional theory (DFT) calculations. Only one conformer of the dimer has been observed in the experiment. DFT/B97-D level calculation shows that N−H···π hydrogen-bonded conformer (T′) is energetically more stable than the N−H···O hydrogen-bonded conformer (HB). Natural bond orbital (NBO) calculation also shows that the hydrogen-bonding interaction in the HB conformer is very weak. Finally, the structure of the observed dimer has been determined to be tilted T-shaped N−H···π hydrogen-bonded (T′) from very excellent agreement between experimental and theoretical N−H stretch frequency. The most significant finding of this study is the first-time observation of a N−H···π bound conformer of a dimer, which wins over a conventional hydrogen-bonded conformer of the dimer.

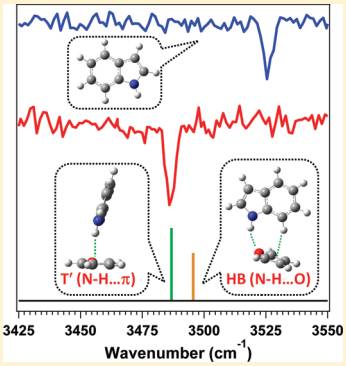


## 1. INTRODUCTION

N−H···π-hydrogen-bonding interaction has received much attention quite recently due to its significant abundance in various biological systems.[1−8] This specific nonconventional hydrogen bonding has become an interesting topic of gas phase spectroscopic study because it has wide variation in the interaction energy, depending on the molecular systems involved. The prototypical example of this type of noncovalent interaction is the benzene···$NH_3$ complex, where the interaction energy is very small ($D_0$ = 1.84 kcal/mol), and this is even smaller than that of benzene···$H_2O$ ($D_0$ = 2.44 kcal/mol).[9−11] On the other hand, very strong N−H···π interaction is observed in the pyrrole dimer, which has a strongly slanted T-shaped geometry with an interplanar angle of 55°.[12] Such a tilted T-shaped geometry compared with the perfect T-shaped one gains maximum stability by effective use of both π-stacking and N−H···π-hydrogen-bonding interactions. Basis set superposition error (BSSE)-corrected binding energy of the pyrrole dimer computed at the MP2 level is about 5.50 kcal/mol, and the observed red shift of the donor N−H stretch is 86 $cm^{-1}$.

There are subsequent studies on N−H···π interactions in various other aromatic dimers. Tilted T-shaped N−H···π bound structure has also been observed for the 2-pyridone···benzene dimer.[13,14] Here, the dimer has a dissociation energy ($D_0$) of 5.17 kcal/mol calculated at the CCSD(T)/aug-cc-pVDZ (aVDZ) level and 56 $cm^{-1}$ of experimental red shift of the N−H stretching frequency. A similar kind of N−H···π interaction has recently been observed in the pyrrole···benzene dimer, in which the observed red shift of the N−H stretch of pyrrole is 59 $cm^{-1}$.[15] The structure of the indole···benzene dimer has been studied by experiment as well as theory, and the dissociation energy of the dimer has been found to be 5.21 kcal/mol.[16−18] Biswal et al. have very recently reported that the indole···benzene dimer has a tilted T-shaped N−H···π bound structure with observed red shift of the N−H stretch frequency of 46 $cm^{-1}$.[19]

It has been concluded from all of these data on N−H···π hydrogen-bonding interaction that this nonconventional hydrogen bond has a strength comparable to a conventional hydrogen bond.[13−15] The conventional hydrogen-bond is defined as X−H···Y, where both X and Y are electronegative atoms (N, O). Given this fact, it will be interesting to ask the question whether a N−H···π hydrogen-bonding interaction can win over conventional hydrogen-bonding interaction. To answer this question, one has to choose a molecular complex, which can exist as a N−H···π bound conformer as well as conventional hydrogen-bonded conformer. Keeping in this mind, we have studied here the indole···furan dimer, which can exist as N−H···π as well as N−H···O bound conformers. The hydrogen-bonded indole···furan dimer is also an interesting molecular system that falls in the category of a special class of mixed complex that is first introduced by our group for the indole···pyridine dimer.[20] A special class of mixed complexes is the dimer, in which the geometry is governed by the subtle balance between conventional hydrogen bonding as well as dispersion interactions. On the other hand, N−H···π bound dimers reported in the literature are defined as mixed complexes, which comprise electrostatic and dispersion interactions as described in the S22 and S66 database of benchmark calculations.[21,22] Here, we have reported the

**Received:** November 25, 2011
**Revised:** January 6, 2012
**Published:** January 9, 2012

investigation of N−H···$\pi$ and N−H···O bound structures of the indole···furan dimer in a supersonic jet by using R2PI, IR-UV double-resonance spectroscopic techniques combined with quantum chemistry calculations.

## 2. METHODS

**2.1. Experimental Section.** The experimental setup has been described in detail elsewhere and is mentioned here briefly.[20] Indole was put in a stainless steel sample holder placed behind a pulsed valve and heated at about 80 °C. The buffer gas argon at a pressure of about 45 psig was bubbled through furan taken in a stainless steel sample container put in a dry ice bath maintained at −78.5 °C. Furan (Sigma Aldrich) vapor seeded in the buffer gas was mixed with indole (Sigma Aldrich) vapor and expanded into the vacuum through a 0.5 mm pulsed nozzle (General valve, series 9, rep. rate 10 Hz). Jet-cooled indole monomer as well as indole···furan heterodimer are ionized using a one-color resonant two-photon ionization (1C-R2PI) technique by frequency-doubled output of a tunable dye laser (ND6000, Continuum) pumped by the second harmonic of a Nd:YAG laser (nanosecond, 10 Hz, Surelite II-10, Continuum). The resolution of the dye laser is ∼0.08 $cm^{-1}$. The typical UV pulse energy used for ionization was ∼0.3−0.4 mJ. The ions were mass-analyzed in the time-of-flight mass spectrometer and detected by a 18-mm-diameter dual MCP detector (Jordan TOF Products) placed at the end of the time-of-flight tube. The ion signal from the detector was amplified using a preamplifier (SRS, model SR445A) and sent to a digital oscilloscope (Tektronix, 350 MHz, DPO 4034) interfaced to a PC via a USB port. Both data acquisition and laser control were performed using home-built LabView-based programs (National Instruments, 8.6 version). For RIDIR spectroscopy, an IR laser was fired 100 ns prior to the UV laser and scanned through the vibrational transitions in the ground electronic state while the UV laser was fixed to a particular transition in the R2PI spectrum of the dimer. The typical pulse energy of the IR laser beam used was about 4−5 mJ. The tunable IR laser is a KTP/KTA-based OPO/OPA (Laser Vision) system pumped by a seeded Nd:YAG laser (nanosecond, 10 Hz, Surelite II-10). The typical resolution of the IR laser used in the experiment is ∼1 $cm^{-1}$. Temporal synchronization among the pulsed valve and various lasers was controlled by using a digital delay generator (BNC, model 575).

**2.2. Computational Section.** Ground state geometry optimizations and harmonic vibrational frequency calculations of various possible conformers of indole···furan dimer were performed at the DFT/B97-D and M05-2X levels using different basis sets. An "ultrafine" numerical integration grid was used for the DFT calculations to obtain reliable results. The binding energies of various conformers of the dimer were corrected for BSSE as well as zero-point vibrational energy (ZPE). BSSE correction was performed using the counterpoise method given by Boys and Bernardi.[23] Natural bond orbital (NBO) analysis for different conformers of the dimer was performed to determine the strength of the hydrogen-bonding interactions present there.[24,25] All calculations were performed using the Gaussian 09 program package.[26] NBO calculations were done by using the NBO program (version 3.1) available in the Gaussian software.[27]

## 3. RESULTS AND DISCUSSION

**3.1. Time of Flight (TOF) Mass Spectrum.** A TOF mass spectrum of the complexes of indole and furan in argon buffer gas recorded at a laser frequency of 35 192 $cm^{-1}$, which corresponds to the electronic origin transition of indole···furan complex, is shown in Figure 1. The mass peak observed at 185 amu is due to the indole···furan dimer, whereas the 253 amu mass peak is designated as the indole···$(furan)_2$ trimer. The mass spectrum also shows higher clusters of indole, that is, $(indole)_2$ and $(indole)_3$, as well as water clusters of indole, that is, indole···$(H_2O)_1$, indole···$(H_2O)_2$, etc.

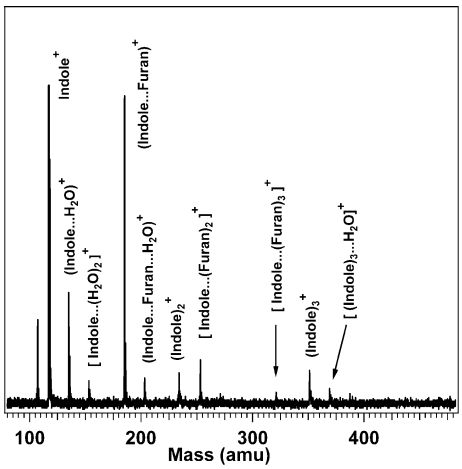


**Figure 1.** TOF mass spectrum of complexes of indole and furan recorded at a laser frequency of 35 192 $cm^{-1}$, which corresponds to the origin band of the indole···furan dimer.

**3.2. Resonant 2-Photon Ionization (R2PI) Spectra.** A one-color R2PI spectrum recorded in the indole···furan dimer mass channel (mass = 185 amu) by cooling furan to dry ice temperature (−78.5 °C) is shown in Figure 2b. The R2PI spectrum of indole is also shown in Figure 2a to compare with the R2PI spectrum in the dimer channel. The origin band ($0_0^0$) for the $S_1 \leftarrow S_0$ electronic transition of indole appears at 35 240 $cm^{-1}$, which matches well with the previous report.[28] The R2PI spectrum in the indole···furan dimer mass channel is measured

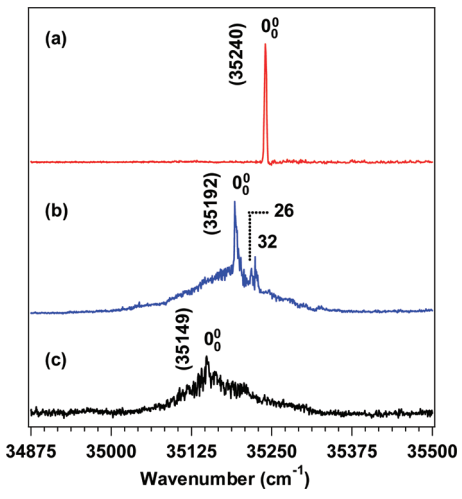


**Figure 2.** One-color R2PI spectra recorded in (a) indole, (b) indole···furan dimer, and (c) indole···$(furan)_2$ trimer mass channels.


dx.doi.org/10.1021/jp211366z | J. Phys. Chem. A 2012, 116, 1368−1374

by electronic excitation of the indole moiety. A very strong, sharp peak observed at 35 192 $cm^{-1}$ in Figure 2b has been assigned as the origin band of the indole···furan dimer. Two relatively weak peaks at $0_0^0$ + 26 and $0_0^0$ + 32 $cm^{-1}$ are assigned as low-frequency intermolecular vibrations of the dimer.

It is quite interesting to compare the red shift in the band origin of the indole···furan dimer with that of related complexes. The red shifts in the $0_0^0$ band of indole···furan, indole···$H_2O$, and *p*-cresol···tetrahydrofuran (THF) complexes are 48, 132, and 482 $cm^{-1}$, respectively.[29−33] Generally, the amount of red shift in the band origin of the complex with respect to that of the monomer indicates the extent of stability of the complex compared with that of the monomer in the excited electronic state. Thus, the $S_1$ state stability of the indole···furan complex studied here is the least compared with that of the other two reported complexes mentioned here.

One characteristic feature of the R2PI spectrum obtained in the dimer mass channel (Figure 2b) is the observation of a very broad background underneath a few sharp peaks. This broad background could be due to origin transitions of multiple conformers of the dimer with their overlapping low-frequency intermolecular vibrations or higher clusters fragmenting into the dimer mass channel. The broadening of the R2PI spectrum could also be due to shortening of the lifetime of the excited state of the dimer through rapid deactivation.

To verify the contribution of the higher clusters in the broadening of the R2PI spectrum measured in the dimer mass channel, we have measured the R2PI spectrum in the indole···$(furan)_2$ trimer mass channel, shown in Figure 2c. Interestingly, the spectrum in the trimer mass channel has also a broad background, which is overlapping to the one observed in the R2PI spectrum in the dimer mass channel. The sharp peak at 35 149 $cm^{-1}$ in the spectrum at the trimer mass is assigned as the origin transition of the indole···$(furan)_2$ trimer. Thus, comparing the R2PI spectra in the dimer and trimer mass channels, it is obvious that the background observed in the spectrum at the dimer mass channel (Figure 2b) is originating mostly from the trimer, which is fragmenting and appearing in the dimer channel. The source of the background in the R2PI spectrum at the dimer mass could also be validated by recording the R2PI spectrum upon increasing vapor pressure (temperature) of furan.

We have recorded the R2PI spectrum of the complex in the dimer mass channel by keeping furan in a bath containing a mixture of dry ice and aqueous solution of $CaCl_2$ to maintain the temperature at approximately −35 °C . The comparison of the R2PI spectra at two different temperatures is depicted in Figure S2 (Supporting Information), which shows that the relative intensity of the sharp features compared with the background in the R2PI spectrum at the dimer mass markedly decreases when the temperature of the furan is increased. This observation reconfirms that the broad background in the R2PI spectrum in the dimer mass channel is mostly due to the higher clusters. To determine whether any other conformer of the dimer contributes to the broad background in the electronic spectrum in the dimer mass (Figure 2b), an IR-UV double-resonance spectroscopy experiment was performed by exciting several positions in the R2PI spectra in both dimer and trimer channels and is discussed in the following section.

**3.3. Resonant Ion Dip InfraRed (RIDIR) Spectra.** Figure 3 shows IR spectra of indole and the indole···furan complex in the N−H stretching region by using RIDIR (resonant ion dip infrared) spectroscopy. The RIDIR spectrum of indole

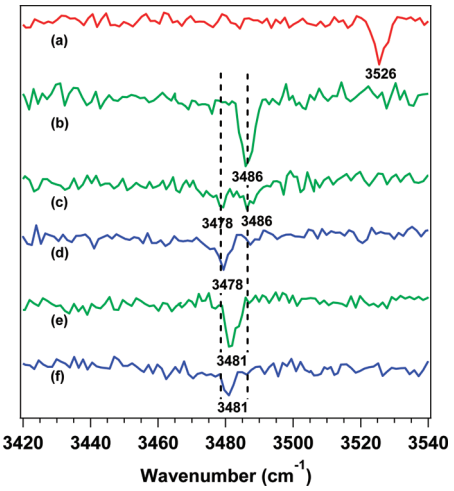


**Figure 3.** RIDIR spectra in the N−H stretching region by probing (a) the $0_0^0$ band of the indole monomer, (b) the $0_0^0$ band of the indole···furan dimer, (c) the 35 149 $cm^{-1}$ band position in the dimer mass channel, (d) the 35 149 $cm^{-1}$ band position in the indole···$(furan)_2$ trimer mass channel, (e) the 35 268 $cm^{-1}$ band position in the dimer mass channel, and (f) the 35 268 $cm^{-1}$ band position in the indole···$(furan)_2$ trimer mass channel.

monomer displayed in Figure 3a exihibits the N−H stretch fundamental at 3526 $cm^{-1}$, which agrees very well with previous reports.[32,34] Figure 3b shows a RIDIR spectrum by probing the origin band of the indole···furan dimer at 35192 $cm^{-1}$. The spectrum shows a single band at 3486 $cm^{-1}$ corresponding to the N−H stretching vibration of the dimer, which is red-shifted by 40 $cm^{-1}$ compared with that of the indole monomer. RIDIR spectra have also been recorded by probing another two sharp but relatively weak peaks at $0_0^0$ + 26 and $0_0^0$ + 32 $cm^{-1}$ in the R2PI spectrum of the dimer. These spectra are shown in Figure S1 of the Supporting Information and are identical to the one shown in Figure 3b. Thus, the peaks at $0_0^0$ + 26 and $0_0^0$ + 32 $cm^{-1}$ are due to low-frequency intermolecular vibration of the dimer.

To shed more light on the origin of the broad background underneath the $0_0^0$ band of the dimer, we have measured the RIDIR spectra by probing several positions on the background of the R2PI spectrum in both dimer and trimer mass channels. For brevity, only a few selected RIDIR spectra by probing the background positions are presented in Figure 3. Figure 3c and d shows RIDIR spectra by probing the 35 149 $cm^{-1}$ position of the broad background in the indole···furan dimer and indole···$(furan)_2$ trimer mass channels, respectively. The spectrum in Figure 3c shows two peaks at 3478 and 3486 $cm^{-1}$, whereas mostly the 3478 $cm^{-1}$ peak is observed in the spectrum displayed in Figure 3d. Thus, it is confirmed that the 35 149 $cm^{-1}$ position of the background obtained in the R2PI spectrum measured in the dimer mass channel originates as a result of overlapping electronic transitions of both the indole···furan dimer and indole···$(furan)_2$ trimer. Similarly, RIDIR spectra were recorded by probing the 35 268 $cm^{-1}$ position of the background of the R2PI spectra in the indole···furan dimer and indole···$(furan)_2$ trimer mass channels and are displayed in Figure 3e and f, respectively. Because both the dimer and trimer IR spectra show a single peak at 3481 $cm^{-1}$, the background observed at 35 268 $cm^{-1}$ in the dimer R2PI spectrum is due to electronic transition of another conformer of the indole···$(furan)_2$ trimer.


dx.doi.org/10.1021/jp211366z | *J. Phys. Chem. A* 2012, 116, 1368−1374

RIDIR spectra similar to the ones in Figure 3c and e have been observed by probing many other background positions of the R2PI spectrum in the dimer mass channel, and these are provided in Figure S3 of the Supporting Information. It is revealed from all the RIDIR spectra that the broad background of the R2PI spectrum in Figure 2b originates as a result of electronic transitions of two conformers of the indole···$(furan)_2$ trimer as well as the single conformer of the mixed dimer. Thus, it is proved that only one conformer of the dimer is observed in the experiment. Generally UV−UV or IR-UV hole-burning spectroscopies are not very suitable for determining the presence of multiple conformers when the R2PI spectrum is very broad. There are many reports in the literature in which multiple RIDIR spectra are recorded by fixing several UV wavelengths of broad R2PI spectra of the complexes to probe the conformational landscape.[35−37] In general, 2-color R2PI spectroscopy is also used to avoid fragmentation of the higher clusters in the dimer mass channel. But we did not obtain any significant amount of 2-color R2PI signal for the indole···furan complex.

It is worth comparing the red shift in the N−H stretch of indole···furan dimer with that of the prototypical N−H···O hydrogen-bonded complex of indole and $H_2O$, which is 89 $cm^{-1}$.[32,34] The indole···THF complex is also a suitable candidate for comparing the N−H···O hydrogen-bonding interaction with that of the dimer studied in this work. Although there is no literature report of an experimental red shift in the N−H stretch frequency of the indole···THF complex, we obtained the corresponding theoretical value of 230 $cm^{-1}$ at the B97-D/aug-cc-pVDZ level of calculation. The optimized structure of the indole···THF complex is provided in Figure S4 of the Supporting Information.

Interestingly, there is a recent report of a *p*-cresol···THF complex in which strong O−H···O hydrogen-bonding interaction with a O−H stretch red shift of 317 $cm^{-1}$ is present.[33] All of these data reveal that hydrogen-bonding interaction in the indole···furan complex is very weak. It is interesting to note that the N−H stretch red shift in the indole···furan dimer (40 $cm^{-1}$) is very much similar to that in the N−H···$\pi$ bound tilted T-shaped indole···benzene dimer (44 $cm^{-1}$).[19] A similar amount of red shifts in the N−H stretch has also been observed for the N−H···$\pi$ hydrogen-bonded, tilted, T-shaped pyridone···benzene (56 $cm^{-1}$) and pyrrole···benzene (59 $cm^{-1}$) dimers.[13,15] This comparison strongly indicates that the geometry of the observed indole···furan dimer may be primarily N−H···$\pi$ hydrogen-bonded rather than N−H···O hydrogen-bonded.

**3.4. Theoretical Results.** *3.4.1. Structures of Indole···Furan Dimer.* To determine the structure of the observed mixed dimer of indole and furan, DFT calculations of various probable conformers of the dimer were performed using B97-D (dispersion-corrected DFT functional) and M05-2X functionals with various basis sets. Figure 4a shows six probable structures of the indole···furan dimer, which are used as input geometries for optimization at various levels of theory. It is interesting to note here that most of the structures of the dimer are stabilized because of multiple types of noncovalent interactions. Structure I is named HB, which is primarily N−H···O hydrogen-bonded. This HB structure gets a unique V-shaped geometry to maximize the stability through additional C−H···$\pi$ and C−H···O interactions. A similar kind of V-shaped geometry has been reported for the phenol dimer as well as the indole···pyridine dimer.[38−43] Both structures II and III are N−H···$\pi$ hydrogen-bonded, but the former has a right-angle, T-shaped geometry (T), and the latter has a tilted, T-shaped geometry (T′).

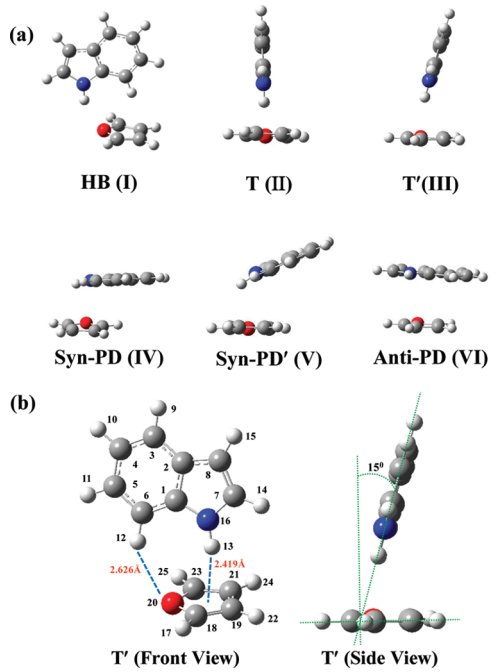


**Figure 4.** (a) Six probable structures of the indole···furan dimer and (b) front and side views of the most stable structure (T′) of the indole···furan dimer optimized at the B97-D/aVDZ level of theory.

It is apparent that the N−H···$\pi$ bound (T and T′) structures are also stabilized through C−H···O and N−H···O interactions. Structures IV, V, and VI are parallel-displaced dimers named as syn-PD, syn-PD′, and anti-PD, respectively. In both the syn-PD and syn-PD′ structures, the indole NH group and oxygen atom of furan are oriented on the same side, but the geometry of the former is nearly parallel, whereas the latter is tilted parallel-displaced. In the case of the anti-PD structure, the indole NH group and oxygen atom of furan are positioned on the opposite side in the parallel fashion.

Both syn-PD and T (right-angle, T-shaped) structures converge to a T′ (tilted T-shaped) structure after optimization at various levels of theory. Thus, six probable structures are converged into four structures after optimization. Initial and final structures of the indole···furan dimer optimized at the B97-D/aVDZ level are provided in Figure S5 of the Supporting Information.

Frequency calculations of all four stable structures have been performed to check whether these are true minima. The N−H···$\pi$ bound tilted T-shaped (T′) structure is the most stable conformer of the indole···furan dimer. Figure 4b shows both front and side views of the T′ structure optimized at the B97-D/aVDZ level of theory. The tilt angle of the T′ structure is 15°; that is, the angle between the molecular planes of indole and furan is 75°. A similar kind of tilted, T-shaped structure has been reported for 2-pyridone···benzene, pyrrole···benzene, indole···benzene, and pyrrole dimers.[12,13,15,19] The tilted T-shaped structure (T′) becomes more stable compared with the right angle T-shaped one (T) as the former maximizes the stability through N−H···$\pi$ as well as weak $\pi$···$\pi$ stacking interactions.

A few selected geometrical parameters of the four stable conformers of the indole···furan dimer are provided in Table 1. Specially, various types of nonbonding interactions present in


dx.doi.org/10.1021/jp211366z | J. Phys. Chem. A 2012, 116, 1368−1374

**Table 1. Selected Geometrical Parameters of Four Conformers of the Indole···Furan Dimer Calculated at the B97-D/aVDZ Level of Theory**

| | T′(NH···π) | HB | syn-PD′ | anti-PD |
|---|---|---|---|---|
| $d_{N-H\cdots O}$ (Å) | 2.843 | 2.224 | 2.772 | |
| $d_{N\cdots O}$ (Å) | 3.63756 | 3.15060 | 3.26816 | |
| $\Delta r_{N-H}$ (Å) | 0.0026 | 0.0015 | 0.0030 | 0.00008 |
| ∠N−H−O | 135.65 | 151.34 | 110.45 | |
| $d_{C-H\cdots O}$ (Å) | 2.62655 | 2.90560 | 4.81976 | |
| ∠C−H−O | 142.52 | 127.01 | 86.96 | |
| $d_{C-H\cdots\pi}$ (Å) | | 2.57670 | 3.87773 | |
| $d_{N-H\cdots\pi}$ (Å) | 2.41981 | 3.14909 | 2.53926 | |

most of the conformers are presented in the table. One important geometric parameter, listed in Table 1, which indicates how strongly the N−H group of indole is involved in the hydrogen-bonding interaction in various conformers of indole···furan dimer is $\Delta r_{N-H}$ (lengthening of N−H bond). $\Delta r_{N-H}$ in the HB structure is 0.0015 Å, whereas that in both T′ and syn-PD′ structures is 0.003 Å. These data clearly point out that hydrogen-bonding interaction in the HB structure is weaker compared with that in the N−H···π bound structures of the indole···furan dimer.

Table 2 presents BSSE- and ZPE-corrected binding energies as well as relative energies of all the four stable conformers of the dimer calculated at various levels of DFT using different basis sets. Because most of the conformers of indole···furan dimer are stabilized by electrostatic as well as dispersion interactions, calculation has been performed using dispersion-corrected DFT functionals such as B97-D and M05-2X. By comparing the binding energies and relative energies of the four conformers of the dimer at various levels of theory, it is clear that the N−H···π bound T′ structure of the dimer is the most stable one.

**Table 2. BSSE- and ZPE-Corrected Binding Energies (kcal/mol) as well as N−H Stretch Frequencies ($cm^{-1}$) of Four Structures of Indole···Furan Dimer Calculated at Various Levels of Theory[a]**

| methods | conformers | $\Delta E_e$ | $\Delta E_0$ | $E_{rel}$ | $\nu_{N-H}$ |
|---|---|---|---|---|---|
| exptl | | | | | 3486 |
| B97-D/LP[b] | HB | −4.605 | −3.883 | 0.389 | 3494 |
| | NH···π (T′) | −4.988 | −4.272 | 0.000 | 3486 |
| | syn-PD′ | −4.882 | −3.960 | 0.312 | 3470 |
| | anti-PD | −3.030 | −2.575 | 1.697 | 3530 |
| B97-D/cc-pVDZ | HB | −4.549 | −3.818 | 0.427 | 3496 |
| | NH···π (T′) | −5.001 | −4.245 | 0.000 | 3485 |
| | syn-PD′ | −4.928 | −4.159 | 0.086 | 3467 |
| | anti-PD | −2.582 | −2.220 | 2.025 | 3530 |
| B97-D/cc-pVTZ | HB | −4.577 | −3.888 | 0.453 | 3505 |
| | NH···π (T′) | −5.077 | −4.341 | 0.000 | 3487 |
| | syn-PD′ | −5.015 | −4.222 | 0.119 | 3475 |
| | anti-PD | −3.053 | −2.677 | 1.664 | 3529 |
| B97-D/aVDZ | HB | −4.603 | −3.913 | 0.346 | 3496 |
| | NH···π (T′) | −4.946 | −4.259 | 0.000 | 3487 |
| | syn-PD′ | −4.848 | −4.117 | 0.142 | 3470 |
| | anti-PD | −2.990 | −2.644 | 1.615 | 3528 |
| M05−2X/cc-pVTZ | HB | −4.007 | −3.403 | 0.049 | 3500 |
| | NH···π (T′) | −3.937 | −3.452 | 0.000 | 3475 |
| | syn-PD′ | −3.897 | −3.326 | 0.126 | 3467 |
| | anti-PD | −1.797 | −1.418 | 2.034 | 3537 |

[a] $\Delta E_e$, BSSE-corrected binding energy; $\Delta E_0$, BSSE- + ZPE-corrected binding energy. $E_{rel}$, ZPE-corrected relative energy of the conformer with respect to the most stable conformer. The N−H stretch frequency of the experimentally observed conformer of the indole···furan dimer is also provided. [b] LP stands for 6-311++G (3df, 3pd) basis set.

It is interesting to note that the difference in the binding energies of HB, T′, and syn-PD′ is quite small. Very recently, it has been reported for the indole···benzene dimer that the N−H stretch frequency is a more sensitive probe for structure determination of the observed conformer of the dimer when multiple conformers are close in energy.[19] We have compared the experimentally observed N−H stretch frequency of the indole···furan dimer with those obtained theoretically for the four conformers, and they are provided in Table 2. Theoretical N−H stretch frequencies of the four conformers of the dimer are corrected using a scaling factor obtained from the ratio of the observed and calculated N−H stretch frequency of indole monomer at every level of theory. The result shows that the observed N−H stretch frequency (3486 $cm^{-1}$) of the dimer matches extremely well with that of the T′ structure calculated at various levels of theory. It is worth mentioning that the result obtained at the DFT-D level is more satisfactory compared with that at the M05-2X level.

Comparison of an experimental IR spectrum of the observed dimer and theoretical IR stick spectra of four conformers of the dimer obtained at the B97-D/aVDZ level of theory is provided in Figure 5. By combining the binding energy as well as the N−H stretch frequency values, it is confirmed that the observed indole···furan dimer has the N−H···π bound T′ structure. It is quite interesting to note that the observed N−H stretch frequency (3486 $cm^{-1}$) of the indole···furan complex is also in close agreement with the experimental N−H stretch frequency (3479 $cm^{-1}$) of the N−H···π bound T′ structure of indole···benzene complex reported by Biswal et al.[19] This comparison reconfirms our proposed assignment of the structure of the observed dimer in our experiment.

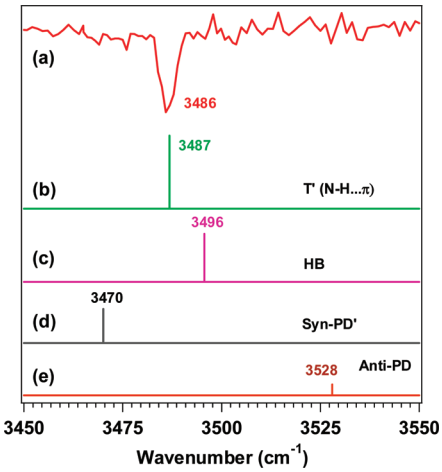


**Figure 5.** (a) RIDIR spectra in the N−H stretching region by probing the origin band of the indole···furan dimer. (b−e) Theoretical IR stick spectra of four conformers of the indole···furan dimer obtained at the B97-D/aVDZ level of theory. Theoretical IR frequencies were scaled by using a scaling factor of 0.9805 obtained from the ratio of experimental and theoretical N−H stretch frequencies of indole monomer.


dx.doi.org/10.1021/jp211366z | J. Phys. Chem. A 2012, 116, 1368−1374

Table 3. Decomposition of Interaction Energies (kcal/mol) in Various Conformers of the Indole···Furan Dimer Calculated at the M05-2X/cc-pVTZ Level of Thoery

| | $\Delta E_{elec}$ | $\Delta E_{ex}$ | $\Delta E_{rep}$ | $\Delta E_{pol}$ | $\Delta E_{disp}$ | $\Delta E_{tot}$ | $\Delta E_{disp}/\Delta E_{ele}$ |
|---|---|---|---|---|---|---|---|
| HB | −4.86 | −2.47 | 11.85 | −1.16 | −7.45 | −4.08 | 1.53 |
| T′ (NH···$\pi$) | −3.84 | −2.28 | 11.30 | −1.21 | −7.97 | −4.00 | 2.07 |
| syn-PD′ | −3.89 | −2.61 | 11.96 | −1.38 | −8.05 | −3.97 | 2.07 |
| anti-PD | −1.45 | −2.84 | 14.25 | −1.05 | −10.72 | −1.81 | 7.39 |

*3.4.2. Energy Decomposition Analysis of the Dimer.* Because various conformers of the dimer studied here consist of multiple types of noncovalent interactions, it is important to know the contribution of different types of interaction energies to the stabilization of the complex. For this purpose, we have used the localized molecular orbital-energy decomposition analysis (LMO-EDA) procedure introduced by Su and Li and implemented in the GAMESS, USA software.[44,45] Table 3 shows the decomposition of the total interaction energy ($\Delta E_{total}$) of various conformers of the dimer into electrostatic ($\Delta E_{elec}$), exchange ($\Delta E_{ex}$), repulsion ($\Delta E_{rep}$), polarization ($\Delta E_{pol}$), and dispersion ($\Delta E_{disp}$) components. The ratios of dispersion to the electrostatic interactions (disp/elec) in all the four conformers are also provided in the table. It is quite interesting to note that the HB conformer is also partially dominated by dispersion interaction like the other three dispersion-dominated conformers. These results strongly indicate that the hydrogen-bonding interaction in the HB conformer is quite weak as it loses to the dispersion interaction. Overall, we can tell that dispersion wins over electrostatics in the indole···furan dimer.

*3.4.3. Natural Bond Orbital Analysis.* For quantitative determination of the strength of the hydrogen bond interaction in the HB and T′ structures of the dimer, NBO analysis was performed at the B97-D/aVDZ level of theory. In the case of the HB structure, hydrogen bond interaction occurs through the charge transfer delocalization of the lone pair orbital of the hydrogen bond acceptor (oxygen atom) over the antibonding orbital of the hydrogen bond donor (N−H group). On the other hand, hydrogen bond interaction in the T′ structure is involved through the delocalization of the $\pi$-orbitals of the hydrogen bond acceptor (furan ring) over the antibonding orbital of the hydrogen bond donor (N−H group). Figure 6 shows the interaction of the NBOs $n_{sp2}(O) \rightarrow \sigma^*_{NH}$ and $n_p(O) \rightarrow \sigma^*_{NH}$ in the HB structure as well as $\pi_{C18-C19}$ (furan) $\rightarrow \sigma^*_{NH}$ and $\pi_{C23-C21}$ (furan) $\rightarrow \sigma^*_{NH}$ in the T′ structure of the dimer.

The NBO delocalization energy is determined by the second order perturbative energy, $E^{(2)}_{i\rightarrow j^*}$, where $i$ and $j^*$ stand for an acceptor and a donor orbital, respectively. Total $E^{(2)}_{i\rightarrow j^*}$ values for the HB and T′ structures are 3.12 and 3.56 kcal/mol, respectively. The NBO results demonstrate that the hydrogen bond interaction in the HB structure is, indeed, very weak. This could be due to a very small $E^{(2)}_{i\rightarrow j^*}$ value (1.16 kcal/mol) for the $n_p(O) \rightarrow \sigma^*_{NH}$ interaction in the HB structure. Actually, the availability of the p-type lone pair on the oxygen atom of furan is less for hydrogen bonding because it takes part in the aromaticity of the furan ring. On the other hand, the $E^{(2)}_{i\rightarrow j^*}$ value for the $n_p(O) \rightarrow \sigma^*_{NH}$ interaction in the hydrogen-bonded structure of the indole···THF complex calculated at the same level of theory (B97-D/aVDZ) is 9.19 kcal/mol. Comparison of various NBO parameters of the indole···THF complex and HB as well as the T′ structures of the indole···furan dimer is provided in Table S1 of the Supporting Information. NBO analysis indeed shows that the occupancy of the p-type lone pair on the oxygen atom in the furan monomer (1.687) is much less compared with that in the THF monomer (1.909). Thus, the NBO analysis supports the interpretation that the observed indole···furan dimer has a N−H···$\pi$ bound tilted T-shaped geometry.

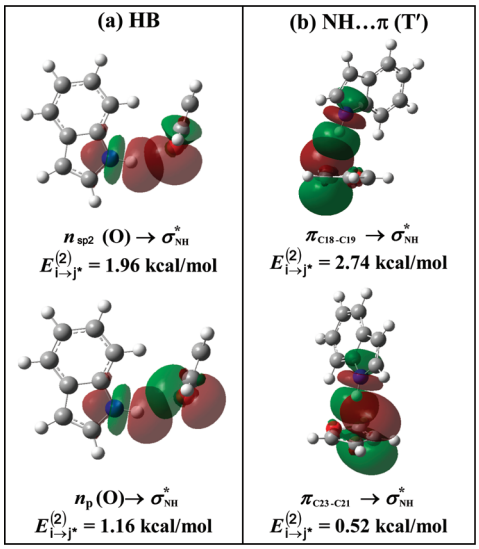


Figure 6. Natural bond orbitals of (a) HB and (b) N−H···$\pi$ (T′) conformers of the indole···furan dimer showing the interactions between hydrogen bond donors and acceptors.

## 4. CONCLUSIONS

In conclusion, R2PI and IR-UV double-resonance spectroscopy experiments as well as DFT calculations have been performed to determine the structure of the observed indole···furan dimer in the supersonic jet. The R2PI spectrum measured in the dimer mass channel shows a broad background with a few sharp features. The RIDIR spectra have been obtained by probing various background positions of the R2PI spectra in the indole···furan dimer as well as the indole···$(furan)_2$ trimer mass channels. The result shows that the major contribution of the broad background in the dimer R2PI spectrum is due to the fragmentation of the indole···$(furan)_2$ trimer. The presence of only one conformer of the dimer is also confirmed in the experiment. The observed dimer has been found to have a N−H···$\pi$ bound, tilted, T-shaped structure by combining the results of experimental as well as theoretical NH stretch frequency, binding energy, and NBO calculations. The current study demonstrates that the N−H···$\pi$ bound structure can win over the conventional N−H···O bound hydrogen-bonded structure.

## ■ ASSOCIATED CONTENT

### Supporting Information

RIDIR spectra by probing the $0^0_0$ + 26 and $0^0_0$ + 32 $cm^{-1}$ bands of the indole···furan dimer, R2PI spectra in the indole···furan


dx.doi.org/10.1021/jp211366z | J. Phys. Chem. A 2012, 116, 1368−1374

dimer mass channel by changing the furan vapor pressure, RIDIR spectra by probing several background positions of the R2PI spectrum of the dimer, optimized structure of the indole···THF complex at the B97-D/aVDZ level of theory, initial and final structures of the indole···furan dimer optimized at the B97-D/aVDZ level, table listing NBO parameters of the HB and T′ conformers of the indole···furan dimer and indole···THF dimer, completed ref 26. This material is available free of charge via the Internet at http://pubs.acs.org.

## AUTHOR INFORMATION

### Corresponding Author

*Phone: 91-20-2590-8078. Fax: 91-20-2586-5315. E-mail: a.das@iiserpune.ac.in, aloke.das73@gmail.com.

## ACKNOWLEDGMENTS

The authors gratefully acknowledge the financial support received from the Indian Institute of Science Education & Research (IISER), Pune to carry out the research. S.K. thanks CSIR for a research fellowship. Research support from the IISER Pune supercomputer facility is also acknowledged. This work is also supported by the Department of Science and Technology, India (Grant No. SR/S1/PC/0054/2010) and DST nanoscience unit of IISER (Grant No. SR/NM/NS-42/2009). The authors acknowledge Dr. Anirban Hazra for fruitful discussions.

## REFERENCES

(1) Desiraju, G. R.; Steiner, T. Oxford University Press, New York, 1999.
(2) Burley, S. K.; Petsko, G. A. *FEBS Lett.* **1986**, *203*, 139.
(3) Levitt, M.; Perutz, M. F. *J. Mol. Biol.* **1988**, *201*, 751.
(4) Steiner, T.; Koellner, G. *J. Mol. Biol.* **2001**, *305*, 535.
(5) Meyer, E. A.; Castellano, R. K.; Diederich, F. *Angew. Chem., Int. Ed.* **2003**, *42*, 1210.
(6) Duan, G.; Smith, V. H.; Weaver, D. F. *J. Phys. Chem. A* **2000**, *104*, 4521.
(7) Hughes, R. M.; Waters, M. L. *J. Am. Chem. Soc.* **2006**, *128*, 13586.
(8) Tóth, G.; Murphy, R. F.; Lovas, S. *J. Am. Chem. Soc.* **2001**, *123*, 11782.
(9) Rodham, D. A.; Suzuki, S.; Suenram, R. D.; Lovas, F. J.; Dasgupta, S.; Goddard, W. A.; Blake, G. A. *Nature* **1993**, *362*, 735.
(10) Mons, M.; Dimicoli, I.; Tardivel, B.; Piuzzi, F.; Brenner, V.; Millie, P. *Phys. Chem. Chem. Phys.* **2002**, *4*, 571.
(11) Courty, A.; Mons, M.; Dimicoli, I.; Piuzzi, F.; Gaigeot, M.-P.; Brenner, V.; de Pujo, P.; Millié, P. *J. Phys. Chem. A* **1998**, *102*, 6590.
(12) Dauster, I.; Rice, C. A.; Zielke, P.; Suhm, M. A. *Phys. Chem. Chem. Phys.* **2008**, *10*, 2827.
(13) Ottiger, P.; Pfaffen, C.; Leist, R.; Leutwyler, S.; Bachorz, R. A.; Klopper, W. *J. Phys. Chem. B* **2009**, *113*, 2937.
(14) Pfaffen, C.; Frey, H.-M.; Ottiger, P.; Leutwyler, S.; Bachorz, R. A.; Klopper, W. *Phys. Chem. Chem. Phys.* **2010**, *12*, 8208.
(15) Pfaffen, C.; Infanger, D.; Ottiger, P.; Frey, H.-M.; Leutwyler, S. *Phys. Chem. Chem. Phys.* **2011**, *13*, 14110.
(16) Braun, J. E.; Grebner, Th. L.; Neusser, H. J. *J. Phys. Chem. A* **1998**, *102*, 3273.
(17) Braun, J.; Neusser, H. J.; Hobza, P. *J. Phys. Chem. A* **2003**, *107*, 3918.
(18) Geng, Y.; Takatani, T.; Hohenstein, E. G.; Sherrill, C. D. *J. Phys. Chem. A* **2010**, *114*, 3576.
(19) Biswal, H. S.; Gloaguen, E.; Mons, M.; Bhattacharyya, S.; Shirhatti, P. R.; Wategaonkar, S. *J. Phys. Chem. A* **2011**, *115*, 9485.
(20) Kumar, S.; Biswas, P.; Kaul, I.; Das, A. *J. Phys. Chem. A* **2011**, *115*, 7461.
(21) Jurecka, P.; Sponer, J.; Cerny, J.; Hobza, P. *Phys. Chem. Chem. Phys.* **2006**, *8*, 1985.
(22) Řezáč, J.; Riley, K. E.; Hobza, P. *J. Chem. Theory Comput.* **2011**, *7*, 3466.
(23) Boys, S. F.; Bernardi, F. *Mol. Phys.* **1970**, *19*, 553.
(24) Weinhold, F.; Landis, C. R. Cambridge University Press: New York, 2005.
(25) Reed, A. E.; Curtiss, L. A.; Weinhold, F. *Chem. Rev.* **1988**, *88*, 899.
(26) Frisch, M. J.; Trucks, G. W.; Schlegel, H. B. *Gaussian09, Revision B.01*; Gaussian, Inc.: Wallingford CT, 2009.
(27) Glendening, E. D.; Reed, A. E.; Carpenter, J. E.; Weinhold, F. *NBO Version 3.1*.
(28) Hager, J. W.; Demmer, D. R.; Wallace, S. C. *J. Phys. Chem.* **1987**, *91*, 1375.
(29) Hager, J.; Ivanco, M.; Smith, M. A.; Wallace, S. C. *Chem. Phys.* **1986**, *105*, 397.
(30) Huang, Y.; Sulkes, M. *J. Phys. Chem.* **1996**, *100*, 16479.
(31) Tubergen, M. J.; Levy, D. H. *J. Phys. Chem.* **1991**, *95*, 2175.
(32) Carney, J. R.; Hagemeister, F. C.; Zwier, T. S. *J. Chem. Phys.* **1998**, *108*, 3379.
(33) Biswal, H. S.; Wategaonkar, S. *J. Chem. Phys.* **2011**, *135*, 134306.
(34) Carney, J. R.; Zwier, T. S. *J. Phys. Chem. A* **1999**, *103*, 9943.
(35) Callahan, M. P.; Gengeliczki, Z.; Svadlenak, N.; Valdes, H.; Hobza, P.; de Vries, M. S. *Phys. Chem. Chem. Phys.* **2008**, *10*, 2819.
(36) Gengeliczki, Z.; Callahan, M. P.; Kabeláč, M.; Rijs, A. M.; de Vries, M. S. *J. Phys. Chem. A* **2011**, *115*, 11423.
(37) Maity, S.; Patwari, G. N.; Sedlak, R.; Hobza, P. *Phys. Chem. Chem. Phys.* **2011**, *13*, 16706.
(38) Felker, P. M. *J. Phys. Chem.* **1992**, *96*, 7844.
(39) Ebata, T.; Watanabe, T.; Mikami, N. *J. Phys. Chem.* **1995**, *99*, 5761.
(40) Weichert, A.; Riehn, C.; Brutschy, B. *J. Phys. Chem. A* **2001**, *105*, 5679.
(41) Hobza, P.; Riehn, C.; Weichert, A.; Brutschy, B. *Chem. Phys.* **2002**, *283*, 331.
(42) Brause, R.; Santa, M.; Schmitt, M.; Kleinermanns, K. *ChemPhysChem* **2007**, *8*, 1394.
(43) Kolaski, M.; Kumar, A.; Singh, N. J.; Kim, K. S. *Phys. Chem. Chem. Phys.* **2011**, *13*, 991.
(44) Su, P.; Li, H. *J. Chem. Phys.* **2009**, *131*, 14102.
(45) Schmidt, M. W.; Baldridge, K. K.; Boatz, J. A.; Elbert, S. T.; Gordon, M. S.; Jesnsen, J. H.; Koseki, S.; Matsunaga, N.; Nguyen, K. A.; Su, S. J.; Windus, T. L.; Dupuis, M.; Montgomery, J. A. *J. Comput. Chem.* **1993**, *14*, 1347.